2005 American Control Conference
June 8-10, 2005. Portland, OR, USA

Image-Based Dynamic Modeling of Thermal Therapies Using Proper Orthogonal Decomposition of Magnetic Resonance Thermometry Images

(Invited Paper)

Ran Niu and Mikhail Skliar

Abstract— **Planning and model-based control of noninvasive thermal therapies require thermal response and power deposition models of the target, which are site- and patient-specific. In this paper, we propose an image-based approach to the identification of low-dimensional model of noninvasive thermal treatments using MRI temperature imaging. The models of thermal response and specific absorption rate (SAR) of noninvasively transduced energy by the target and the surrounding normal tissue are identified in the reduced basis of proper orthogonal decomposition of thermal images. The developed methods are less sensitive to temporal and spatial noises in image data, slow image acquisition rate, and are suitable for adaptive model re-identification by recursively utilizing newly acquired images. The proposed concepts and developed methods are tested using the results of MR thermal imaging experiments with tissue phantom noninvasively heated by focused ultrasound.**

I. Introduction

Thermal treatments have shown promises in noninvasive medical interventions, such as tumor ablation [1], and as an adjuvant treatment to radio- and chemotherapies [2]. Noninvasive heating also creates the possibility of thermally activated, targeted drug delivery [3]. To be effective, thermal treatments must selectively heat the target (e.g., tumor) without excessively elevating the temperature of the surrounding healthy tissue [4].

The monitoring of temperatures in the tumor and surrounding healthy tissues is critically important to achieve objectives of thermal therapies. Traditional invasive temperature monitoring techniques use catheterized thermal probes to obtain measurements in a few fixed spatial locations. In addition to the problem of causing patient's pain and discomfort, the invasive probes may interference with the noninvasive heating of the tissue, and can alter the energy absorption in the target. Such limitations of the traditional monitoring methods make noninvasive temperature measurements highly desirable.

In recent years, magnetic resonance imaging (MRI) has gained an importance as a promising noninvasive temperature monitoring method. MRI can provide both detailed anatomical information for target definition and the detailed temperature maps of the selected two-dimensional slices. In fact, comprehensive three-dimensional temperature measurements are available, constrained only by technological limitations and long scan time to achieve high signal-to-noise measurements. A number of magnetic resonance temperature mapping methods [5], [6], [7] have been investigated. Several methods were evaluated and compared based on the results of phantom experiments [8], where it was concluded that water proton resonance frequency (PRF) method is the most suitable for MR monitoring of small temperature changes ($< 1°$C) during thermal treatments.

Model-based planning and control of thermal therapies are essential in achieving the desired treatment outcome. With the use of treatment models, the optimization of the treatment plan becomes possible, and may include the patient- and site-dependent selection of appropriate noninvasive actuators and their spatial positioning, and the configuration of the temperature monitoring system. The model-based real-time control of treatments has significant advantages over the traditional methods. In particular, using the model predictive control the desired thermal dose may be delivered to the tumor without exceeding the maximum allowable temperature in the critical normal tissues close to the treatment site [9], [10]. Unfortunately, modeling of the thermal treatments presents difficulties. For example, the first-principle modeling leads to high-dimensional models, which makes the model-based feedback control of thermal treatments computationally demanding, or even infeasible. First-principle models also depend on parameters, such as blood perfusion, which often can only be estimated or measured with high uncertainty

The MRI thermometry gives us the ability to acquire noninvasive spatially distributed temperature measurements anywhere in the target. In this paper, we outline a novel approach to image-based, low-dimensional modeling and identification of thermal therapies. The identification starts with pre-treatment experiments during which the MR thermal images, characterizing the response of the target and the surrounding tissue to thermal excitation, are collected. The excitation is applied using the same noninvasive transducer, which will later be used to administer the actual therapy. The proper orthogonal decomposition (POD) of collected images is used to obtain the orthonormal basis of empirical eigenfunctions, which are then used to identify low-dimensional patient- and site-specific projection models of thermal therapies and specific absorption rate of the tissue. The developed methods are validated using experimental results of MRI thermal imaging of the tissue phantom during focused ultrasound heating.

II. Proper Orthogonal Decomposition of Images

The proper orthogonal decomposition is a technique often used to extract a set of basis functions for an approximate,

This work was supported by the NIH and NSF, grants NCI-R01-CA33922 and CTS 0117300.

R. Niu and M. Skliar are with the Department of Chemical Engineering, University of Utah. Correspondence to mikhail.skliar@utah.edu

modal-like representation of an infinite-dimensional, distributed parameter system (DPS). Generally, a numerical solution of partial differential equation(s) at different times is used as an input to the POD algorithm to produce the desired basis functions. It was previously shown [11] that POD is the most efficient way to obtain dominant modes of an infinite-dimensional dynamical system. The identified basis can then be used in combination with the projection methods to obtain a finite-dimensional approximation of the original infinite-dimensional DPS model.

In this paper, the POD method is used to identify an orthonormal basis of infinite-dimensional system based on the measurements in the form of a time series of images, rather than the results of numerical solution of the known PDE model. A brief outline of the POD in the context of this paper is given next. For more detailed discussion, see [11], [12], [13], [14].

Let $S = \{U_i(r) : 1 \leq i \leq N, r \in \Omega\}$ be the set of N images (or snapshots) taken at arbitrary instants of time, which characterize the evolution of a distributed parameter physical process defined on the spatial domain Ω. The problem is to obtain a function $\phi(r)$, which is the best at characterizing the spatial distribution of the process based on the available ensemble of snapshots U_i. Mathematically, the problem is to find $\phi(r)$, such that the projections of all snapshots $U_i(r)$ onto function $\phi(r)$ has, on average, the maximum possible value:

$$\max_{\phi} \lambda = \frac{1}{N} \sum_{i=1}^{N} \frac{< U_i, \phi >^2}{< \phi, \phi >} \tag{1}$$

Here $<f, g>= \int_\Omega f(r)g(r)dr$ denotes the inner product of two square integrable functions over domain Ω. To ensure uniqueness of the solution, the normalization condition of $< \phi, \phi >= 1$ is imposed.

Define $R \equiv \int_\Omega K(r, r')dr'$, where

$$K(r, r') = \frac{1}{N} \sum_{i=1}^{N} U_i(r)U_i(r') \tag{2}$$

Then the right hand side of (1) can be expressed compactly as

$$\int_\Omega \{R\phi\}\{\phi\}dr =< R\phi, \phi > \tag{3}$$

which makes it clear that the maximization problem (1) is equivalent to the following eigenvalue problem:

$$R\phi = \lambda\phi \tag{4}$$

Namely, function ϕ that maximizes the objective function (1) is the eigenfunction of (4) corresponding to the largest eigenvalue λ.

Solution of the eigenproblem (4) may be difficult to find. Following [15], assume that eigenproblem (4) has N solutions each expressed as

$$\phi_k = \sum_{i=1}^{N} \omega_i^k U_i(r), \quad k = 1, \ldots, N \tag{5}$$

where the coefficients ω_i^k are the components of the eigenvector $W_k = [\omega_1^k \ldots \omega_N^k]^T$ found from the matrix eigenproblem

$$CW_k = \lambda_k W_k \tag{6}$$

where C is a nonnegative covariance matrix of available images:

$$C = [c_{ij}],\ c_{ij} = \frac{1}{N} \int_\Omega U_i(r)U_j(r)dr,\ i, j = 1, .., N \tag{7}$$

Because of the symmetry of K, all eigenvalues λ_k are real and nonnegative and the eigenvectors of the Hermitian matrix C corresponding to distinct eigenvalues are orthogonal. It is also assumed that all λ_k's are in descending order. The normalization condition of eigenvectors W_k is satisfied by requiring $< W_k, W_k >= \frac{1}{N\lambda_k}$. The resulting basis $\Phi = \{\phi_1, \phi_2, \ldots, \phi_N\}$ is the orthonormal basis of the sequence of images S.

The amount of information captured by the projection of the set S on the i-th eigenfunction is characterized by the corresponding eigenvalue, which means that ϕ_1 captures the most information about spatial distribution of the snapshot ensemble, followed by ϕ_2 as the next most informative direction, and so on. Therefore, the eigenvalues can be used as a guidance in selecting the order of the reduced order POD basis for the set S. For instance, we can select the order M of the reduced basis Φ such that the predetermined level $0 < e \leq 1$ of the total energy of the snapshot ensemble is captured. For example, the problem may be to select the smallest M such that $\frac{\sum_{i=1}^{M} \lambda_i}{\sum_{i=1}^{N} \lambda_i} > e$, where e is specified. It was reported [16] that in many cases the values of λ_i decay rapidly and $M \ll N$ even for e close to 1.

The obtained reduced order basis $\{\phi_j(r)\}_{j=1}^{M}$ can be used to obtain a low-dimensional projection model relating the time history of process inputs to the temporal evolution of snapshots. In the subsequent discussion, the basis $\{\phi_j(r)\}_{j=1}^{M}$ is used to: (a) Represent thermal MRI images in the reduced form, which is, in essence, an image compression operation; (b) Identify low-dimensional thermal response models of the thermal treatments and (c) Estimate the SAR of the ultrasound transducer, which, generally, is patient- and site-specific.

III. Traditional Model of Thermal Therapies

First-principle model of the heat transfer in tissues is given by convection-diffusion partial differential equation, which depends on the geometry and inhomogeneity of the domain, the distribution of blood vessels, the corresponding blood flow rates, thermal conductivity and power deposition in the tissue. Direct measurement of blood flow and other needed model parameters is difficult, which motivated the introduction of simplified models, such as the following Pennes' bioheat transfer equation (BHTE) [17]:

$$\rho C \frac{\partial T}{\partial t} = \nabla \cdot (k\nabla T) - W_b C_b (T - T_a) + Q \tag{8}$$

with initial conditions $T(r, 0) = T_a$, where T (°C) is the temperature response, Q (W/m^3) is the power deposited in

the tissue, ρ (kg/m^3) and k (W/m°C) are the tissue density and thermal conductivity, C and C_b are the specific heats of tissue and blood (in J/kg°C) respectively, W_b ($kg/m^3 s$) is the blood-perfusion related parameter, and T_a is the arterial (equilibrium) temperature.

IV. Image Reduction, Treatment Modeling and Parameter Identification

A. POD Basis Functions and Image Modeling

Consider a series of MRI thermal images $T(r,t_k)$ of the spatial domain of interest $r \in \Omega$ collected at N sampling moments t_k. The images, acquired at pre-treatment stage in response to mild thermal excitation by the transducer to be later used during the actual therapy, forms the snapshot set S. The reduced set of empirical eigenfunctions $\Phi = \{\phi_j : j = 1,\dots,M\}$, found by solving the eigenvalue problem (6), forms the orthonormal basis of the image space. In reduced basis of M elements, image $T(r,t)$ is approximated by $T_p(r,t)$ as

$$T(r,t) \approx T_p(r,t) = \sum_{j=1}^{M} \phi_j(r)\hat{T}_j(t) \tag{9}$$

where M is selected to achieve the desired accuracy of approximation. The data communication between the MRI scanner and the thermal treatment controller, which uses thermal images in the feedback, requires that only a M-dimensional vector of projections $\hat{T}(t)$ is exchanged, thus reducing data traffic and computer storage requirements. The same reduced basis is also used to represent the power deposition Q (in W/m^3):

$$Q(r,t) \approx Q_p(r,t) = \sum_{j=1}^{M} \phi_j(r)\hat{u}_j(t) \tag{10}$$

generated by the energy transducer.

In the subsequent experiments, more than 300 pixels of an MRI thermal image, which would traditionally be treated as independent pointwise measurements, describe the thermal response in the spatial region of interest around the focal zone of ultrasound transducer. We show that this measurement information can be adequately approximated with a single identified eigenfunction ($M = 1$). Therefore, the POD image approximation allows us to reduce the communication traffic between the MRI scanner and the treatment controller $\sim$ 300-fold with little loss of useful information.

B. Projection Model of the Thermal Response

Assume that the bioheat equation is the appropriate model of the thermal response. The subsequent development can be easily modified for a different form of the distributed parameter thermal response model. In particularly, it can be adapted for the case of the convection-diffusion model. To obtain the weak Galerkin formulation with the reduced POD basis, use (9) and (10) in the Pennes' model (8). After taking the inner product with all basis functions $\phi_i(r)$ obtain

$$\dot{\hat{T}}_i(t) = \sum_{j=1}^{M} < \phi_i(r), \alpha(r)\nabla^2\phi_j(r) - \beta(r)\phi_j(r) > \hat{T}_j(t) + \sum_{j=1}^{M} < \phi_i(r), \gamma(r)\phi_j(r) > \hat{u}_j(t) \tag{11}$$

where $\alpha(r) = \dfrac{k}{\rho C}$, $\beta(r) = \dfrac{W_b C_b}{\rho C}$, $\gamma(r) = \dfrac{1}{\rho C}$. Equation (11) gives a low M-dimensional projection model of the thermal response. In compact form, the projection model (11) can be written as

$$\dot{\hat{T}} = A\hat{T}(t) + B\hat{u}(t) \tag{12}$$

where $A = [a_{ij}]$, $B = [b_{ij}]$, $i,j = 1,\dots,M$ and the elements of A and B are given by the following expressions:

$$a_{ij} = <\phi_i(r), \alpha(r)\nabla^2\phi_j(r)> - <\phi_i(r), \beta(r)\phi_j(r)> \tag{13}$$

$$b_{ij} = <\phi_i(r), \gamma(r)\phi_j(r)> \tag{14}$$

If all coefficients of the Pennes' model are known or independently identified, then the projection model (12) is a computationally inexpensive way to predict thermal response of the patient, which makes it well suited for the use in model-based control of thermal therapies.

Next, we develop the method for identification of the projection model (12) directly from available thermal images. The identified projection model is independent of the assumed form of the partial differential models. If its relationship with the PDE model is established, the identified projection model can be used to estimate unknown parameters of the governing model; for example, M^2 equations (13) can be used to identify unknown parameters of the Pennes' equation.

C. Identification of Projection Model

The SAR pattern which characterizes energy absorption by the target is site- and patient-specific and, therefore, *a priori* unknown for even well-characterized transducer. As a consequence, an unusual feature of the model identification problem at hand from the system identification perspective is the need to identify the system matrix A of the thermal response model (12) without knowing thermal input to the process. Our approach, therefore, is to use thermal images acquired during tissue cooling, when the transducer is switched off, to first identify A, and then use the result to identify thermal input $B\hat{u}$.

Temperature decay is described by the following projection model:

$$\dot{\hat{T}}(t) = A\hat{T}(t) \tag{15}$$

We wish to estimate matrix A such that 2-norm of the error between the measured T_m, and the predicted tissue cooling temperatures is minimized, on average, for each moment the measurement is available:

$$\min_A \|T_m(r,t) - T_p(r,t)\|_2 \tag{16}$$

Here the model prediction is $T_p(r,t) = \mathbf{\Phi}(r)\hat{T}(t)$, where $\mathbf{\Phi} = [\phi_1(r)\ \phi_2(r) \cdots \phi_M(r)]$, and $\hat{T}$ must satisfy equation (15). For a single measurement at time t_k, the solution of the optimization problem (16) with the equality constraints (15) gives that A must satisfy:

$$T_m(r,t_k) = \mathbf{\Phi}(r)e^{At_k}\hat{T}_0 \tag{17}$$

where $\hat{T}_0$ is the initial condition for the projection model (15), calculated so that $\mathbf{\Phi}(r)\hat{T}_0$ gives the best approximation of the temperature distribution $T(r,t)$ at the time when cooling begins. The differentiation of (17) yields

$$Ae^{At_k}\hat{T}_0 = \mathbf{\Psi}\mathbf{\Phi}^T T_t(r,t_k) \tag{18}$$

where $T_t(r,t_k)$ is the time derivative of the temperature measurements $T_m(r,t_k)$ and the matrix pseudo inverse $\mathbf{\Psi} = (\mathbf{\Phi}^T\mathbf{\Phi})^\dagger$. For a single measurement at t_k, the combination of (17) and (18) after obvious manipulations gives the following linear system of equations:

$$T_m^T(r,t_k)\mathbf{\Phi}\mathbf{\Psi}^T A^T = T_t^T(r,t_k)\mathbf{\Phi}\mathbf{\Psi}^T \tag{19}$$

where $T_t^T(r,t_k)\mathbf{\Phi}\mathbf{\Psi}^T$ is the $1 \times M$ row vector.

To account for all available measurements during the tissue cooling, introduce the following matrices of measurements and their derivatives: $\boldsymbol{T}_m = [T_m(r,t_1)\cdots T_m(r,t_n)]$ and $\boldsymbol{T}_t = [T_t(r,t_1)\cdots T_t(r,t_n)]$. Then the system matrix A that solve the identification problem is found as a (least squares) solution of the following matrix equation:

$$\boldsymbol{T}_m^T\mathbf{\Phi}\mathbf{\Psi}^T A^T = \boldsymbol{T}_t^T\mathbf{\Phi}\mathbf{\Psi}^T \tag{20}$$

The proposed batch identification method, which finds A as the solution of (20), can be re-formulated in a recursive form, enabling a continuous adaptation of A based on MRI thermal images acquired during the actual treatment. This is an important capability since blood perfusion and tissue properties are known to change in response to elevated temperatures.

D. SAR Identification

The power deposition pattern for a given transducer or applicator is traditionally identified using linear slope method [18], an approach known to be sensitive to the measurement noise and slow sampling rate. The alternative proposed here is less affected by random spatial and temporal disturbances, relatively slow acquisition rate of MRI thermometry and is well-suited for the image-based identification of the SAR.

For known tissue density, the SAR (in W/kg) is related to the power deposition as

$$SAR(r,t) = \frac{Q(r,t)}{\rho(r)} \tag{21}$$

The SAR identification is posed as the following constrained optimization problem:

$$\min_{\hat{u}} \parallel T_m(r,t) - T_p(r,t) \parallel_2 \tag{22}$$

where T_m is the measured temperature, T_p is given by equation (9) and the projected states must satisfy model equation (12). The system matrix A of the projection model is identified following the method of Section IV-C. Since B (cf. equation 14) depends only on the identified eigenfunctions and the relatively well-known and little-changing tissue density and heat capacity (both often assumed equal to the water values), matrix B in the projection model is considered to be known. Similarly to the interpretation of $\hat{T}$ as temperature projections, and with the reference to equation (10), the vector $\hat{u}(t)$ can be viewed as the projection of the transducer power deposition $Q(r,t)$ into the space with $\{\phi_j\}_{j=1}^M$ as the basis. The problem (22) is now to find projection $\hat{u}(t)$ such that when used in the model equation (12), the predicted $\hat{T}$ minimize the error between the measured and the predicted temperatures (9). Once $\hat{u}(t)$ is found, the estimated power deposition and SAR patterns is given by equations (10) and (21).

Consider the identification of $\hat{u}$ under the assumption that $T_m(r,t)$ is the measured evolution of the temperature distribution in response to the step change ($\hat{u} = cont$) in transducer power. Using the analytical prediction of the temperature response in the projected space, for a single temperature measurement $T_m(r,t_k)$, the minimal (zero) prediction error is obtained if $\hat{u}$ satisfies the following equation:

$$\mathbf{\Phi}(r)(e^{At_k} - I)A^{-1}B\hat{u} = T_m(r,t_k) - \mathbf{\Phi}(r)e^{At_k}\hat{T}_o \tag{23}$$

where $\hat{T}_o$ is the projected initial temperature before the step change in power is applied. After assembling equations (23) for all available measurements into a single system of equations, obtain that $\hat{u}$ must satisfy the following equation:

$$\mathbf{\Phi}\begin{bmatrix} e^{At_1} - I \\ \vdots \\ e^{At_N} - I \end{bmatrix} A^{-1}B\hat{u} = \begin{bmatrix} T_m(r,t_1) \\ \vdots \\ T_m(r,t_N) \end{bmatrix} - \mathbf{\Phi}\begin{bmatrix} e^{At_1} \\ \vdots \\ e^{At_N} \end{bmatrix}\hat{T}_o \tag{24}$$

where the matrix pseudo-inverse should be used if A is not invertible. If the domain is initially at thermal equilibrium, then equation (24) is simplified by setting $\hat{T}_o = 0$.

The solution of the SAR identification problem (22) is the least squares solution of the assembled system of equations (24). The sensitivity of the identified $\hat{u}$ to temporal measurement noises is reduced as the number of measurements is increased. The effect of zero-mean spatial noises in thermal images can be reduced by using the following projection form of equation (24):

$$\begin{bmatrix} e^{At_1} - I \\ \vdots \\ e^{At_N} - I \end{bmatrix} A^{-1}B\hat{u} = \begin{bmatrix} \hat{T}_m(t_1) \\ \vdots \\ \hat{T}_m(t_N) \end{bmatrix} - \begin{bmatrix} e^{At_1} \\ \vdots \\ e^{At_N} \end{bmatrix}\hat{T}_o \tag{25}$$

where the vector of measurement projections is found from equation $\mathbf{\Phi}(r)\hat{T}_m(t) = T_m(r,t)$. The estimates of the power deposition $Q(r,t)$ and the corresponding SAR are obtained by using the identified $\hat{u}(t)$ in equations (10) and (21).

The SAR and Q identified following the described method are for a single and constant level of transducer power. If SAR changes linearly with power, as often the case during low-intensity treatments, then the SAR for different power levels is obtained by correspondingly scaling a single identified power distribution $Q(r)$.

V. Materials and Methods

A. MR Thermometry

The water PRF shift is temperature dependent and can be used to calculate the phase difference of two gradient-echo images [7]. To obtain a temperature map during thermal treatment, phase images are obtained and subtracted from the baseline phase image to yield the phase difference $\triangle\phi$ at each scan time. The relative temperature difference $\triangle T$ is calculated as

$$\triangle T = \frac{\triangle\phi}{\gamma_g \cdot \alpha \cdot B_0 \cdot TE} \tag{26}$$

where α is the temperature dependent PRF change coefficient for aqueous tissue, γ_g is the gyromagnetic ratio, B_0 is the main magnetic field strength, TE is the echo time for the phase accumulation.

B. Experimental Setup

The experiment is performed using Siemens Trio 3 Tesla MRI Scanner. The ultrasound field is generated by a single, spherically focused, air backed transducer, with a resonant frequency of 1.5 MHz. Its aperture diameter is 10cm and radius of curvature ∼18cm. The transducer was placed in a bath containing degassed and deionized water. The in-house built, MRI-compatible ultrasound positioning system is used to move the position of the focal zone. In current experiments, after initial alignment the transducer position remained fixed. The transducer is driven by the function generator (Stanford Research System, Sunnyvale, CA, model DS345), amplified using RF amplifier (ENI Inc, Rochester, NY, model A150). The electrical impendence of the transducer is matched to the output impendence of the amplifier by an external LC matching circuit.

A cubic $11 \times 11 \times 11$cm agar phantom is used during the experiments. Figure 1 shows the temperature image in the focal plane with phantom appearing as rectangular object above the ultrasound positioning system. Dark (red) region inside the phantom is the area of elevated temperature (gradient scale is in °C). We select the region of interest (ROI) as the region of an appreciable temperature elevation, which has pixel coordinates of $62 \leq x \leq 72$ and $50 \leq x \leq 78$. On the line of focal symmetry ($x = 67$), the maximum temperature rise of 12.5°C in response to a step change in transducer power is observed.

Gradient-echo sequences with the following acquisition parameters are used to obtain MRI temperature images: repetition time =75ms, echo time TE=10ms, field of view 30×30cm, flip angle 25°, scan time 10s. The overall image size is 128×128 pixels, voxel size is 2.3×2.3×2mm. In our experiment, the phase difference of two consecutive complex images are used to calculate the temperature difference, where $\alpha = -0.01\text{ppm}\cdot C^{-1}$ [19] is assumed.

VI. Results

A step increase of 3.1W of ultrasound power is applied for 893s and then switched off to the original zero level. The total duration of MR temperature measurements is 1037 seconds. A total of 109 MR thermal images are collected with 10s interval. The image data in the ROI are used to identify eigenfunctions. Figure 2 shows the first four empirical eigenfunctions within the ROI of 11×29 pixels identified using all available thermal images. Since the first eigenfunction captures approximately 98.19% of the information carried by the collection of 109 images, the projection model with a single state $\hat{T}$ is used to model the process. Figure 3 compares the MRI measurement at $t = 893s$, time when the peak temperature elevation was observed, with the model prediction based on the single-state projection model. The prediction error is also shown. A very good agrement with measurements is evident; Figure 4, which shows the predicted and measured temperature evolution in four different locations on the line of focal symmetry $x = 67$, further confirms this conclusion. Finally, Figure 5 shows the power deposition pattern $Q(r)$ within the ROI identified with a single eigenfunction. As expected for unperfused phantom, the temperature distribution, the first identified eigenfunction and the power deposition pattern are similar in shape.

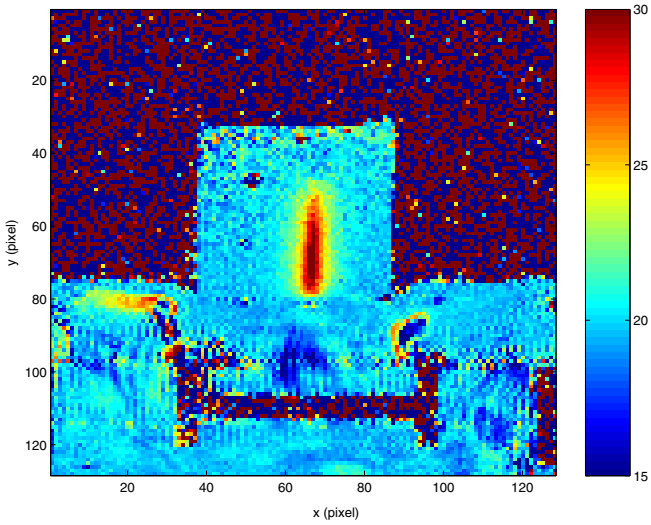

Fig. 1. MRI temperature map of agar phantom heated by focused ultrasound transducer.

VII. Conclusions

We have developed a methodology for image-based reduced-order modeling and identification of distributed parameter systems, and demonstrated its application to the case of noninvasive thermal therapies. The results of experimental study using MRI thermometry of tissue phantom during focused ultrasound heating confirm that the method is well-suited for the identification of the reduced-order SAR and dynamic thermal response models of clinically relevant targets and real-time compression of MRI thermometry images. Our current effort is directed at the development of efficient treatment controllers that utilize low-dimensional projection models and use thermal images in the feedback. Though our emphasis is on thermal therapies, the developed approach has a broader applicability in image-based identification of distributed parameter systems.

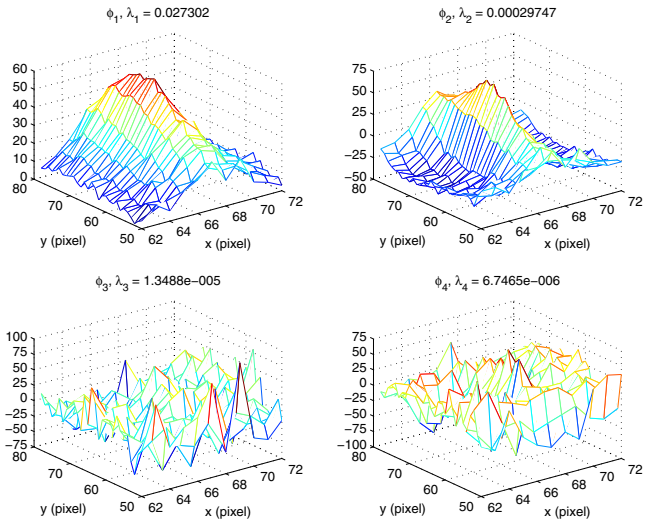

Fig. 2. Leading eigenfunctions identified using MR thermal images. ϕ_1 and ϕ_2 capture 98.19% and 1.07% of information within the ROI, respectively.

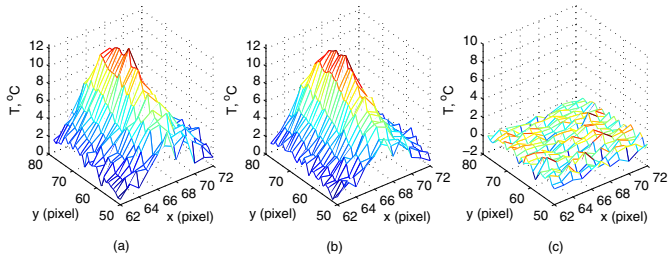

Fig. 3. Temperature elevation: (a) measured; (b) predicted; (c) prediction error.

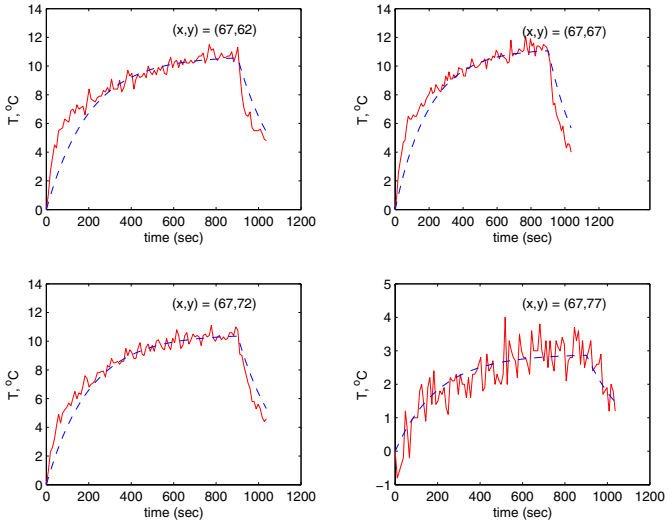

Fig. 4. Evolution of temperature elevation at different positions on the line of focal symmetry.

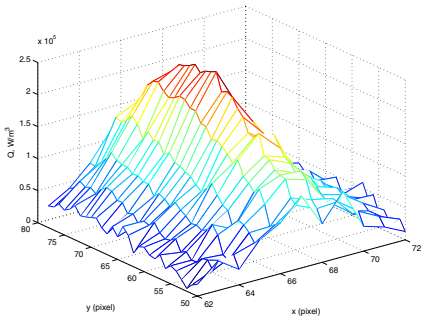

Fig. 5. Identified power deposition pattern with $M = 1$.

REFERENCES

[1] H.E. Cline, J.F. Schenck, K. Hynynen, R.D. Watkins, S.P. Souza, and F.A. Jolesz. MR-guided focused ultrasound surgery. *J Comput Assist Tomogr*, 16:956–965, 1992.

[2] M.W. Dewhirst and P.K. Sneed. Those in gene therapy should pay closer attention to lessons from hyperthermia. *Int. J. Radiat. Oncol. Biol. Phys.*, 57:597–599, 2003.

[3] K. Kakinuma, R. Tanaka, H. Takahashi, Y. Sekihara, M. Watanabe, and M. Kuroki. Drug delivery to the brain using thermosensitive liposome and local hyperthermia. *Int. J. Hyperthermia*, 12:157–165, 1996.

[4] R.B. Roemer. Engineering aspects of hyperthermia therapy. *Annu. Rev. Biomed. Eng.*, 01:347–376, 1999.

[5] H.E. Cline, K. Hynynen, C.J. Hardy, R.D. Watkins, J.F. Schenck, and F.A. Jolesz. MR temperature mapping of focused ultrasound surgery. *Magn Reson Med*, 31:628–636, 1994.

[6] D.Le Bihan, J. Delannoy, and R.L. Levin. Temperature mapping with MR imaging of molecular diffusion: application to hyperthermia. *Radiology*, 171:853–857, 1989.

[7] Y. Ishihara, A. Calderon, H. Watanabe, K. Okamoto, Y. Suzuki, K. Kuroda, and Y. Suzuki. A precise and fast temperature mapping using water proton chemical shift. *Magn. Reson. Med.*, 34:814–823, 1995.

[8] W. Wlodarczyk, M. Hentschel, P. Wust, R. Noeske, N. Hosten, H. Rinneberg, and R. Felix. Comparison of four magnetic resonance methods for mapping small temperature changes. *Phys. Med. Biol.*, 44:607–624, 1999.

[9] D. Arora, M. Skliar, and R.B. Roemer. Model-predictive control of hyperthermia treatments. *IEEE Trans. Biomed. Eng.*, 49:629–639, 2002.

[10] D. Arora, M. Skliar, and R.B. Roemer. Minimum-time thermal dose control of thermal therapies. *IEEE Trans. Biomed. Eng.*, 52:191–200, 2005.

[11] P. Holmes, J. Lumley, and G. Berkooz. *Turbulence, Coherent Structures, Dynamical Systems and Symmetry*. Cambridge University Press, Cambridge, 1996.

[12] H.M. Park and D.H. Cho. The use of the Karhunen-Loeve decomposition for the modeling of distributed parameter systems. *Chemical Eng. Sci.*, 51:81–98, 1996.

[13] L. Sirovich. *New Perspectives in Turbulence*. Springer-Verlag: New York, 1991.

[14] S.S. Ravindran. A reduced-order approach for optimal control of fluids using proper orthogonal decomposition. *Int. J. for Numerical Methods in Fluids*, 34:425–448, 2000.

[15] L. Sirovich. Turbulence and the dynamics of coherent structures: Part i-iii. *Quart. Appl. Math.*, 45:561–590, 1987.

[16] M.D. Gunzburger. *Perspectives in Flow Control and Optimization*. SIAM, Philadelphia, 2003.

[17] H.H. Pennes. Analysis of tissue and arterial blood temperatures in resting human forearm. *J. Appl. Physiol.*, 1:93–122, 1948.

[18] R.B. Roemer, A.M. Fletcher, and T.C. Cetas. Obtaining local SAR and blood perfusion data from temperature measurements: Steady state and transient techniques compared. *Int. J. Radiation Oncology Biol. Phys.*, 11:1539–1550, 1985.

[19] R.D. Peters, R.S. Hinks, and R.M. Henkelman. Ex vivo tissue-type independence in proton-resonance frequency shift MR thermometry. *Magn Reson Med*, 40:454–459, 1998.